JOURNAL OF THERMOPHYSICS AND HEAT TRANSFER
Vol. 16, No. 3, July–September 2002

Thermal Periodic Contact of Exhaust Valves in Spark Ignition Air-Cooled Engines

I. Paradis* and J. R. Wagner†
Clemson University, Clemson, South Carolina 29634-0921
and
E. E. Marotta‡
IBM, Poughkeepsie, New York 12601

Internal combustion engines generate exhaust gases at extremely high temperatures and pressures. As these heated gases exit through the exhaust valve, the valve and valve seat insert achieve comparable temperatures. To avoid damage, heat is transferred from the exhaust valve to the valve seat insert as they come into contact with each other during the opening and closing cycle. Modern engine management systems regulate the thermal process through coolant and/or airflow rates, fuel injection, and ignition timing, and exhaust gas recirculation contributions to achieve satisfactory tradeoffs between power, emissions, and efficiency for various engine speeds and loads. One of the primary functions of the engine control unit is the prevention and detection of abnormal combustion to prevent severe engine damage. The online estimation of cylinder component temperatures offers an opportunity for greater engine control measures. A nonlinear dynamic thermal model is presented to describe the transient and steady-state phenomena in the engine's cylinder using a lumped parameter resistance–capacitance network. The model prediction of the engine's thermal behavior establishes a foundation to explore thermal periodic contact issues. Representative experimental and numerical results will be presented and discussed.

Nomenclature

A = state matrix, cross-sectional area
A_{c1} = internal surface area of lower section of the cylinder wall, m^2
A_{c1e} = external surface area of the lower section of the cylinder wall exposed to air, m^2
A_{c1o} = surface area of wall exposed to oil, m^2
A_{c2} = internal surface area of middle section of the cylinder wall, m^2
A_{c2e} = external surface area of middle section of the cylinder wall exposed to air, m^2
A_{c3} = internal surface area of upper section of the cylinder wall, m^2
A_{c3e} = external surface area of upper section of the cylinder wall exposed to air, m^2
A_{ev} = surface area of exhaust valve face exposed to combustion chamber, m^2
$A_{ev\text{-}con}$ = exhaust valve heat transfer contact area, m^2
A_{evf} = surface area of exhaust valve fillet, m^2
A_{ex} = internal surface area of exhaust port of head exposed to exhaust gas, m^2
A_{gasket} = surface area of head gasket, m^2
A_{Hin} = internal surface area of intake port of head exposed to intake gas, m^2
A_{Hm} = surface area of head middle section, m^2
A_{hf} = surface area of head finned body, m^2
A_{hv} = area heat travels through in head, m^2
A_{iv} = surface area of intake valve face exposed to combustion chamber, m^2
A_{ivf} = surface area of intake valve fillet, m^2
A_{oil} = surface area of oil exposed to oil pan, m^2
A_{pistc} = surface area of piston exposed to combustion chamber, m^2
A_{pisto} = piston surface area exposed to oil bath, m^2
A_{pistw} = surface area of piston exposed to cylinder wall, m^2
A_{R5} = surface area between intake port of head exposed to intake gas and head middle section, m^2
A_{R13} = surface area between exhaust node on head and head middle section, m^2
A_{R26} = surface area between upper and middle nodes on the cylinder wall, m^2
A_{R27} = surface area between middle and lower nodes of the cylinder wall, m^2
A_s = surface area, m^2
A_{tube} = surface area of head tubes, m^2
A_{vc} = surface area of valve cover, m^2
A_{vg} = cross-sectional area of valve guide, m^2
A_{vs} = cross-sectional area of valve stem, m^2
B = input matrix
C = output matrix, thermal capacitance
C_{comb} = capacitance of the combustion gases, J/K
C_{c1} = capacitance of the lower node on the cylinder wall, J/K
C_{c2} = capacitance of the middle node on the cylinder wall, J/K
C_{c3} = capacitance of the upper node on wall, J/K
C_{ev} = capacitance of the exhaust valve, J/K
C_{ex} = capacitance of the exhaust gases, J/K
C_{Hex} = capacitance of exhaust node on head, J/K
C_{Hin} = capacitance of intake node on the head, J/K
C_{Hm} = capacitance of middle node on head, J/K
C_{in} = capacitance of incoming fuel/air mix, J/K
C_{iv} = capacitance of the intake valve, J/K
C_{oil} = capacitance of the oil, J/K
C_{pist} = capacitance of the piston, J/K
C_∞ = capacitance of the ambient air, J/K
c_p = specific heat

Presented as Paper 2000-0878 at the 38th Aerospace Sciences Meeting, Reno, NV, 10–13 January 2000; received 18 December 2000; revision received 13 November 2001; accepted for publication 14 November 2001.

*Research Assistant, Automotive Research Laboratory, Department of Mechanical Engineering.
†Assistant Professor, Automotive Research Laboratory, Department of Mechanical Engineering.
‡Senior Engineer/Scientist, Product Packaging, Power and Cooling Group. Senior Member AIAA.

$c_{p\,\mathrm{comb}}$ = specific heat of the combustion gas, J/kg · K
$c_{p\infty}$ = specific heat of the ambient air, J/kg · K
D = output matrix, $R^{p\times m}$
e = elemental errors
h = thermal convection coefficient
h_{comb} = convection coefficient of combustion gas, W/m^2 · K
h_{contact} = periodic contact conductance, W/m^2 · K
h_{ex} = convection coefficient of exhaust gases, W/m^2 · K
h_{hf} = convection coefficient of ambient air and finned portion of head, W/m^2 · K
h_{in} = convection coefficient of incoming fuel mixture, W/m^2 · K
h_{oil} = convection coefficient of piston to oil, W/m^2 · K
h_{op} = forced convection coefficient of ambient air and oil pan, W/m^2 · K
h_{tube} = convection coefficient of ambient air through head tubes, W/m^2 · K
h_{∞} = convection coefficient of ambient air, W/m^2 · K
K = combustion air-to-fuel ratio correction factor
k = thermal conductivity
k_{cyl} = thermal conductivity of cylinder wall, W/m · K
k_{gas} = thermal conductivity of combustion gas, W/m · K
k_{gasket} = thermal conductivity of head gasket, W/m · K
k_{head} = thermal conductivity of cylinder head, W/m · K
k_{valve} = thermal conductivity of valves, W/m · K
k_{vg} = thermal conductivity of valve guide, W/m · K
L = length, m
L_{gasket} = length between cylinder wall and head, m
L_{hv} = characteristic length heat travels in head, m
L_{R5} = length between intake port of head exposed to intake gas and head middle section nodes, m
L_{R13} = length between exhaust node on head and head middle section nodes, m
L_{R26} = length between upper-middle wall nodes, m
L_{R27} = length between middle-lower cylinder wall nodes, m
L_{vg} = thickness of valve guide, m
L_{vs} = characteristic length valve heat travel, m
m = mass, kg
$\dot{m}_a$ = air mass flow rate, kg/s
$\dot{m}_{\mathrm{fuel}}$ = fuel mass flow rate, kg/s
$\dot{m}_{\mathrm{gas}}$ = total gas mass flow rate, kg/s
$\dot{m}_{\mathrm{A/F}}$ = air/fuel mixture mass flow rate, kg/s
N = engine speed, rpm
Q = heat transfer, W
Q_{comb} = heat energy produced by combustion, W
Q_{contact} = valve seat heat transfer, W
Q_{in} = heat flowing to the exhaust valve, W
Q_{low} = heat of combustion of gasoline at air-to-fuel ratio equal to 14.7, J/kg
Q_{out} = heat flowing from the exhaust valve, W
Q_{vg} = valve guide heat transfer, W
R = resistance
R_1 = resistance between ambient air and intake node, K/W
R_2 = resistance between intake side of head and intake node, K/W
R_3 = resistance between intake valve and intake node, K/W
R_4 = resistance between intake valve and intake part of head, K/W
R_5 = resistance between middle part and intake part of head, K/W
R_6 = resistance between combustion gases and intake valve, K/W
R_7 = resistance between combustion gases and middle part of head, K/W
R_8 = resistance between combustion gases and exhaust valve, K/W
R_9 = resistance between ambient air and exhaust node, K/W
R_{10} = resistance between exhaust part of head and exhaust node, K/W
R_{11} = resistance between exhaust valve and exhaust node, K/W
R_{12} = resistance between exhaust valve and exhaust part of head, K/W
R_{13} = resistance between middle part and intake part of head, K/W
R_{14} = resistance between ambient air and intake part of head, K/W
R_{15} = resistance between ambient air and middle part of head, K/W
R_{16} = resistance between ambient air and exhaust part of head, K/W
R_{17} = resistance between middle part of head and upper part of cylinder wall, K/W
R_{18} = resistance between combustion gases and exhaust node, K/W
R_{19} = resistance between combustion gas and piston, K/W
R_{20} = resistance between piston and oil, K/W
R_{21} = resistance between combustion gas and upper part of cylinder wall, K/W
R_{22} = resistance between combustion gas and middle part of cylinder wall, K/W
R_{23} = resistance between piston and middle part of cylinder wall, K/W
R_{24} = resistance between piston and lower part of cylinder wall, K/W
R_{25} = resistance between oil and lower part of cylinder wall, K/W
R_{26} = resistance between upper part and middle part of cylinder wall, K/W
R_{27} = resistance between middle part and lower part of cylinder wall, K/W
R_{28} = resistance between ambient air and upper part of cylinder wall, K/W
R_{29} = resistance between ambient air and middle part of cylinder wall, K/W
R_{30} = resistance between ambient air and lower part of cylinder wall, K/W
R_{31} = resistance between ambient air and oil, K/W
R_{contact} = periodic resistance of valve seat, K/W
Re_{comb} = Reynolds number for combustion gases
R_r = resistance of piston rings, K/W
T_{c1} = lower cylinder wall temperature, K
T_{c2} = middle cylinder wall temperature, K
T_{c3} = upper cylinder wall temperature, K
T_{comb} = combustion gas temperature, K
T_{ev} = exhaust valve temperature, K
T_{ex} = exhaust gases temperature, K
T_{Hex} = head exhaust section temperature, K
T_{Hin} = head intake section temperature, K
T_{Hm} = head middle section temperature, K
T_{in} = intake gases temperature, K
T_{init} = initial temperature, K
T_{iv} = intake valve temperature, K
T_{oil} = oil temperature, K
T_{pist} = piston temperature, K
T_{∞} = surrounding or ambient air temperature, K
t = time, s
t_f = simulation end time, min
$\boldsymbol{u}$ = input vector
w_{R_8} = uncertainty in R_8
w_{pcr} = periodic contact resistance uncertainty
$\boldsymbol{x}$ = state vector
$\dot{x}$ = time derivative of state vector
$\boldsymbol{y}$ = output vector
ΔN = speed increment
ΔT = temperature difference, K
Δt = integration time step
ε = emissivity
$\varepsilon_{\mathrm{comb}}$ = emissivity of the combustion gases
$\varepsilon_{\mathrm{cyl}}$ = emissivity of the cylinder wall

ε_{head} = emissivity of the head
ε_{pist} = emissivity of the piston
θ = crank angle, deg
λ = air-to-fuel ratio
μ_{gas} = gas viscosity, m^2/s
ν = frequency, 1/s
σ = Stefan–Boltzmann constant, $W/m^2 \cdot K^4$

I. Introduction

INTERNAL combustion spark ignition engines ignite a cylinders' air–fuel mixture, toward the end of the compression stroke, to start the combustion process. In carburetor or fuel-injected engines, the gasoline is introduced into the intake airstream above the manifold or near the intake valve. This air–fuel mixture then flows into the cylinder when the intake valve is open. The combustion event generates gases at extremely high temperatures and pressures, which transfer heat to the cylinder walls, piston, cylinder head, lubricating oil, and valves. As these heated gases exit through the exhaust valve, the valve/valve seat insert achieve comparable temperatures. To avoid damage, heat is transferred from the exhaust valve to the valve seat insert as they come into contact with each other during the opening and closing cycle. The engine control unit (ECU) monitors the coolant temperature, engine load, throttle position, engine speed, and knock sensor to regulate the fuel, spark, and cooling processes (e.g., Kelly and Shannon[1]). The thermal management system for air- and liquid-cooled engines relies heavily on forced convection heat transfer with secondary conduction and radiation contributions to maintain an operating temperature within a specified range (e.g., Heywood[2]). For air-cooled engines (Fig. 1), cooling fins are manufactured into the cylinder head. A fan, or flywheel with blades to create an impeller, is attached to the crankshaft and forces inlet air through the engine compartment, or shroud, to remove heat generated during the combustion process. In this configuration, the fan's speed is directly dependent on the engine's speed, which leaves little opportunity to adjust the airflow rate per operational needs without the introduction of an additional engine actuator. In liquid-cooled engines, the heat removed is transferred to the coolant, which circulates near the valve seat insert and throughout the block. In a similar fashion, heat is removed from the cylinder wall and head to the coolant. The internal combustion engine thermal management system is evolving through the application of smart thermostats and variable speed centrifugal water pumps (e.g., Visinic[3] and Wagner et al.[4]).

To better regulate the engine's thermal efficiency, the ECU must have available a model that estimates the thermal behavior of engine cylinder components.[5] In other words, this can permit the realization of higher operating temperatures within the cylinder for greater overall engine efficiency without damaging components. Therefore, a mathematical model must exist that describes the thermal dynamics of the exhaust valve, that is, hottest cylinder component, with attention focused on the periodic contact resistance at the valve–cylinder head interface. In this research, a nonlinear mathematical model was developed to study the thermal behavior of internal combustion engine components for improved temperature control. An important contribution will be the investigation of surface contact resistance at the exhaust valve interface.

The paper is organized as follows. In Sec. II, a literature survey of thermal periodic contact is presented. A lumped parameter thermal model for the engine cylinder is introduced in Sec. III to predict the thermal behavior of exhaust valves. In Sec. IV, experimental and numerical results are presented and discussed for a spark ignition utility engine operating at various speeds under load. The investigation of periodic contact resistance is presented in Sec. V with an analysis that deducts the thermal periodic contact resistance from numerically and experimentally gathered data for specific engine locations. Finally, Sec. VI provides a summary.

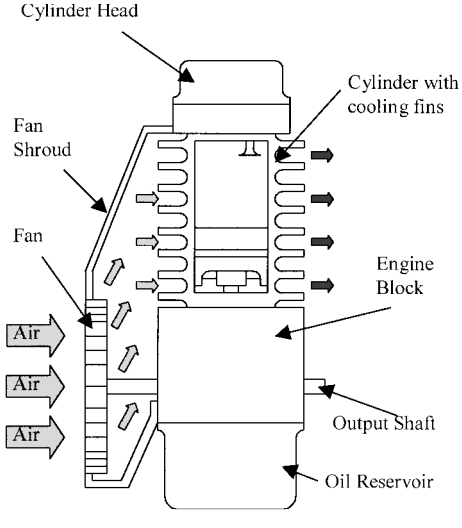

Fig. 1 Air-cooled internal combustion engine thermal system.

II. Literature Survey on Periodic Contact

The contacts between the valve seat insert with the block and exhaust valve bevel with the valve seat insert of an internal combustion engine, shown in Fig. 2, utilized extensively in aluminum engines, present a significant barrier to heat rejection. Heat transfer across pressed junctions, for example, the valve seat insert/engine block junction, is restricted because the real contact area is only a small percentage of the apparent contact area, due to surface irregularities such as surface roughness, limit contact to a relatively few small spots. As a result, heat is constrained to pass primarily through narrow bridges of contact between the two surfaces. This constriction is made evident by the significant change in temperature across the interface of the two surfaces.

When the exhaust valve bevel comes into contact with the valve seat insert, a temperature drop occurs across the interface as a result of surface imperfections. Because of the periodic cycle of contact and the imperfections of the contact, the thermal contact resistance plays an important role in determining the amount of heat transferred from the exhaust valve to the valve seat insert and then to the engine

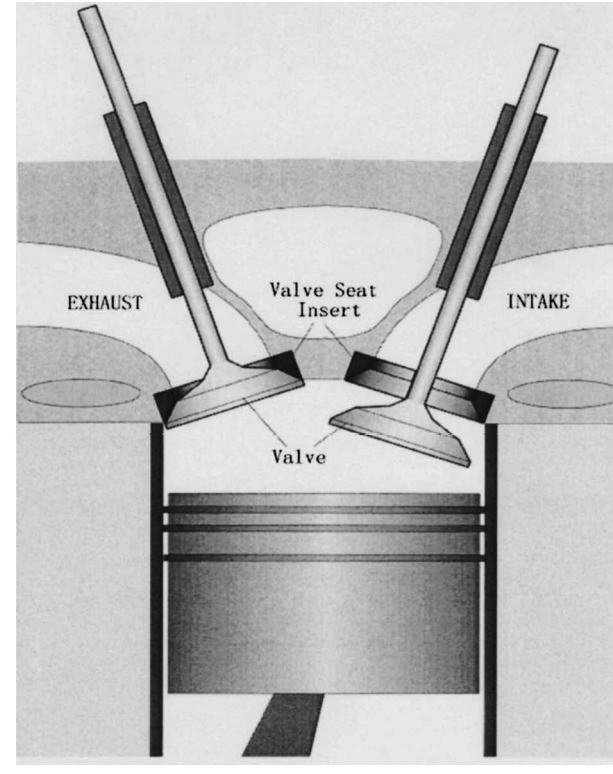

Fig. 2 Configuration of valve seat and engine block contact (Marotta et al.[20]).

block and coolant. The heat transfer rate from the exhaust valve to the valve seat insert also determines the overall temperature of the valve, which subsequently dictates the overall efficiency of the engine. It would be desirable to operate engines at higher temperatures while maintaining the exhaust valve temperature as low as possible to prevent surface ignition phenomena, increase fuel economy and engine performance, lower exhaust emissions, and enhance engine efficiency.

During the past three decades, the problem of heat transfer between two periodically contacting bodies has been the subject of a number of theoretical and experimental investigations. Theoretical studies with the assumptions of plane contact, low frequency of contact, and quasi-steady periodic state under perfect contact were conducted by Reed and Mullineux,[6] Howard and Sutton,[7] and Mikhailov[8] to predict contact conductance at these interfaces. In later studies, Vick and Ozisik[9] and Flach and Ozisik[10] employed the inverse heat conduction method for predicting time-dependent thermal contact conductance from temperature measurements taken within the mediums.

Huang and Ju[11] employed the conjugate gradient method to solve the inverse problem to determine the periodic thermal contact conductance as a function of time between the exhaust valve and seat. The conjugate gradient method utilizes ideas based on variational principles, which transforms one complex inverse problem into three simple problems that can then be solved using standard finite difference techniques. Results indicate that the conjugate gradient method requires only a few iterations to obtain the inverse solution without any prior knowledge of the functional form of the unknown quantity and that the solution is insensitive to the measurement error of the installed thermocouples.

Howard[12] and Moses and Johnson[13] conducted an experimental study of heat transfer through periodically contacting surfaces under the assumptions of imperfect contact and constant thermal contact conductance. Howard's study[12] describes experiments conducted in which heat was transferred through the interface between two solids that were alternately brought into contact and then separated in a continuous cycle. Their results showed that, despite large variations in thermal contact resistance arising from the periodic contact, their earlier theoretical work could predict the average contact resistance due to periodic heat flow at the surfaces.

Couedel et al.[14] conducted an experimental study, which measured in situ the temperature fields under periodic contact for an actual valve–seat configuration. Their experimental parameters included periodic frequencies that ranged between 5 and 25 Hz, which corresponds to engine speeds between 600 and 3000 rpm. The results from their experimental setup indicated that the thermal contact conductance was highly dependent on the rotational frequency of the internal combustion engine and that the mean (time-averaged) and periodic temperature fields can be measured by the use of an integrating voltmeter and extremely fast (response time) instrumentation. In addition, the thermocouples must be positioned close to the valve–seat interface to obtain efficient measurement of the oscillating temperature fields.

The thermal contact resistance for two solids in permanent contact can be estimated from data that include thermal and mechanical properties. These data may include such parameters as surface profiles and material hardness, data on the interface temperature, the apparent interface pressure that may exist, and data on the interstitial fluid, which may be applied at the interface. From this information, an estimate of the thermal contact resistance of the interface in permanent contact can be made. Fenech and Rosenhow,[15] Fenech et al.,[16] Fletcher and Gyorog,[17] Cooper et al.,[18] and Thomas and Probert[19] have conducted these studies. Marotta et al.[20] experimentally examined the usefulness of sintered copper coatings hot pressed onto sintered ferrous valve inserts for enhancement of the thermal contact conductance at the contact between the valve seat insert and the block of an internal combustion engine.

To date, a comprehensive model to predict the heat transfer rate across these junctions (periodic and permanent contacts) for an internal combustion engine either does not exist or is not readily available due to its proprietary nature, that is, the prediction of dynamic real contact area. Therefore, it is clear that, to improve ultimately the engine's performance and fuel efficiency, the heat transfer rate across these junctions becomes of paramount importance. In addition, integration of this thermal information for an online estimation, that is, ECU-based calculations, of the in-cylinder temperatures will help to better regulate the cooling system for enhanced operating temperatures without damage.

III. Engine Cylinder Thermal Model

A mathematical model is presented to describe the thermal behavior of the engine's cylinder components arising from the combustion process. A variety of researchers have proposed dynamic models, including Shayler et al.,[21] who derived and validated a lumped capacity engine block and head model to study temperature, heat flow, and friction characteristics during warm up. Kaplan and Heywood[22] also developed a detailed lumped capacitance computer model using resistor–capacitor thermal networks to study the engine's warm-up process. Bohac et al.[23] presented a comprehensive resistor–capacitor (RC) mathematical model to describe the the engine and exhaust system, as well as physically estimate the gas-to-combustion thermal resistances. Maloney and Olin[24] developed pneumatic and thermal state estimators for engine control; however, the thermal model only considered four lumped capacitance, for example, intake manifold, cylinder head, engine block, and exhaust system. However, little attention has been focused on integrating a detailed description of the periodic contact resistance at the exhaust valves into a lumped capacitance thermal model to support online temperature estimation. In other words, the transient and steady-state heat transfer in internal combustion spark ignition air-cooled engines will be modeled to observe the temperature of cylinder components.

To describe the thermal behavior, a lumped parameter RC network modeling strategy has been applied to the engine's cylinder-head assembly. One of the advantages of a lumped capacitance C, that is, single temperature for each node, and resistance R, that is, conduction, convection and radiation, formulation is the realization of a nonlinear state-space representation. Table 1 lists the thermal resistances and capacitance (refer to Incropera and DeWitt[25]). Note that the thermal model's effectiveness and accuracy is dependent on the number of nodes, which help assure the Biot number criteria.

The thermal model has been developed for the air-cooled engine cylinder system shown in Fig. 3a. Bohac et al.[23] had developed their thermal network for a water-cooled engine. This diagram presents a cross-sectional view of the cylinder, displaying the piston, cylinder wall, cylinder head, valves, spark plug, and oil reserve. The principal engine components (e.g., cylinder wall, engine head, intake and exhaust valves, piston, oil, surrounding air, and gases in the inlet, exhaust, and undergoing combustion) have been selected as nodes for the thermal model. The corresponding lumped capacitance, that is, single temperature for each node, and resistance network has been constructed in Fig. 3b to describe the thermal paths in the engine. The heat transfer between these nodes can be written as a set of nonlinear differential equations.

The node designated as T_{comb} represents the combustion gas temperature, and the governing equation becomes

$$C_{\text{comb}}\frac{\mathrm{d}T_{\text{comb}}}{\mathrm{d}t} = -\frac{1}{R_6}(T_{\text{comb}} - T_{\text{iv}}) - \frac{1}{R_7}(T_{\text{comb}} - T_{\text{Hm}}) - \frac{1}{R_8}(T_{\text{comb}} - T_{\text{ev}}) - \frac{1}{R_{18}}(T_{\text{comb}} - T_{\text{ex}}) - \frac{1}{R_{19}}(T_{\text{comb}} - T_{\text{pist}}) - \frac{1}{R_{21}}(T_{\text{comb}} - T_{c3}) - \frac{1}{R_{22}}(T_{\text{comb}} - T_{c2}) + Q_{\text{comb}} \tag{1}$$

where Q_{comb} is the heat supplied to the cylinder by the combustion and, in some descriptions, friction processes. This supplied energy can be expressed either empirically (e.g., Taylor and Toong[26]) or analytically, respectively, as

$$Q_{\text{comb}} = 10.4\pi B k_{\text{gas}}(T_{\text{comb}} - T_{\text{oil}})\left(\frac{\dot{m}_{\text{fuel}}(1 + \text{AFR})}{\pi\mu_{\text{gas}}B}\right)^{0.75} \tag{2a}$$

Table 1 Summary of thermal resistances and capacitance components

Thermal component	Expression
Conduction resistance	$\{L/Ak\}$
Convection resistance	$\{1/hA_s\}$
Radiation resistance	$\left\{\frac{T_i - T_j}{A_s \sigma \varepsilon F_{ij}\left(T_i^4 - T_j^4\right)}\right\}$
Capacitance	mc_p

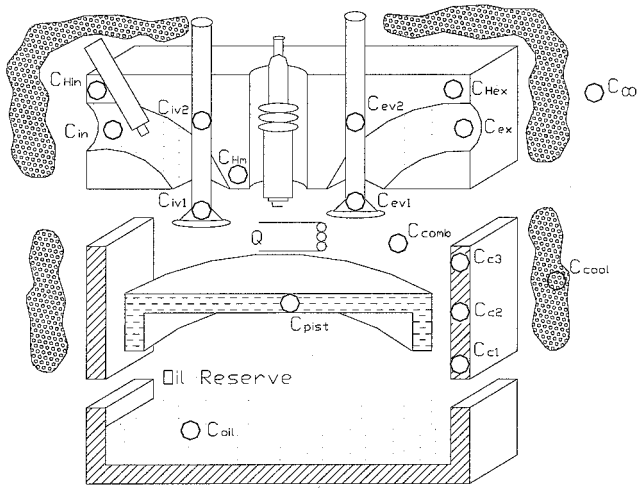

a) Nodal component diagram

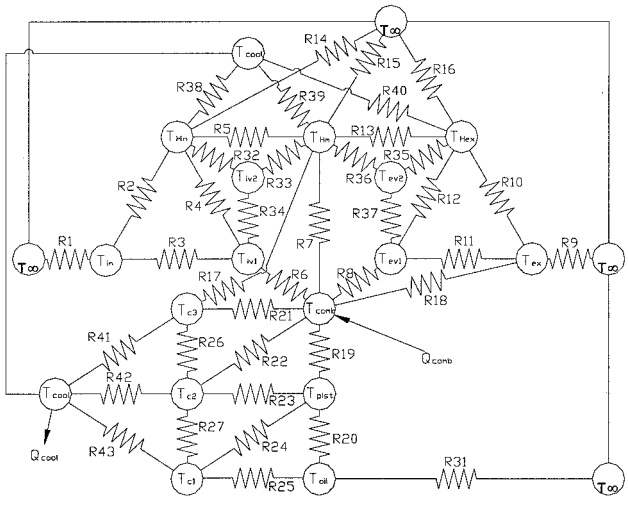

b) RC network schematic

Fig. 3 Air-cooled engine.

$$Q_{\text{comb}} = K\dot{m}_{\text{fuel}} Q_{\text{low}} \tag{2b}$$

The variable air-to-fuel ratio (AFR), or λ, is the air-to-fuel ratio of the mixture entering the engine cylinder. The correction factor was first incorporated by Yoo et al.,[27] which for this study was incorporated into the lumped model, and was methodologically determined to match the analytical lump model results to the experimentally gathered data. Therefore, an expression for the correction factor K may be written as

$$K = \text{rpm}/2000 + 1.65 \tag{2c}$$

where 1.64 is the load-dependent factor and 2000 corresponds to the operating speed. In this analysis, Eq. (2b) will be pursued with the assumption of stoichiometric conditions, that is, AFR = 14.7. Each of the resistances, that is, R_{6-8}, R_{18}, R_{19}, R_{21}, and R_{22}, describes the mode of energy transfer between the combustion node and the corresponding engine components. For instance, the resistor describing the energy transfer between the combustion gases and the piston is R_{19}. This resistor represents two parallel resistances that correspond to convection and radiation heat transfer modes described by Eq. (20d).

The inlet air–fuel mixture and the exhaust gases flowing in/out of the engine nodes T_{in} and T_{ex} may be expressed as

$$C_{\text{in}}\frac{dT_{\text{in}}}{dt} = -\frac{1}{R_1}(T_{\text{in}} - T_\infty) - \frac{1}{R_2}(T_{\text{in}} - T_{\text{Hin}}) - \frac{1}{R_3}(T_{\text{in}} - T_{\text{iv}}) \tag{3}$$

$$C_{\text{ex}}\frac{dT_{\text{ex}}}{dt} = -\frac{1}{R_9}(T_{\text{ex}} - T_\infty) - \frac{1}{R_{10}}(T_{\text{ex}} - T_{\text{Hex}}) - \frac{1}{R_{11}}(T_{\text{ex}} - T_{\text{ev}}) - \frac{1}{R_{18}}(T_{\text{ex}} - T_{\text{comb}}) \tag{4}$$

The engine cylinder head may be partitioned into three sections, for example, inlet, middle, and exhaust sides, based on the incoming gas flow, combustion process, and exhaust gas flow. The equations for these nodes become

$$C_{\text{Hin}}\frac{dT_{\text{Hin}}}{dt} = -\frac{1}{R_2}(T_{\text{Hin}} - T_{\text{in}}) - \frac{1}{R_4}(T_{\text{Hin}} - T_{\text{iv}}) - \frac{1}{R_5}(T_{\text{Hin}} - T_{\text{Hm}}) - \frac{1}{R_{14}}(T_{\text{Hin}} - T_\infty) \tag{5}$$

$$C_{\text{Hm}}\frac{dT_{\text{Hm}}}{dt} = -\frac{1}{R_5}(T_{\text{Hm}} - T_{\text{Hin}}) - \frac{1}{R_7}(T_{\text{Hm}} - T_{\text{comb}}) - \frac{1}{R_{13}}(T_{\text{Hm}} - T_{\text{Hex}}) - \frac{1}{R_{15}}(T_{\text{Hm}} - T_\infty) - \frac{1}{R_{17}}(T_{\text{Hm}} - T_{c3}) \tag{6}$$

$$C_{\text{Hex}}\frac{dT_{\text{Hex}}}{dt} = -\frac{1}{R_{10}}(T_{\text{Hex}} - T_{\text{ex}}) - \frac{1}{R_{12}}(T_{\text{Hex}} - T_{\text{ev}}) - \frac{1}{R_{13}}(T_{\text{Hex}} - T_{\text{Hm}}) - \frac{1}{R_{16}}(T_{\text{Hex}} - T_\infty) \tag{7}$$

The following two differential equations represent the energy exchange that occurs at the intake and exhaust valve nodes:

$$C_{\text{iv}}\frac{dT_{\text{iv}}}{dt} = -\frac{1}{R_3}(T_{\text{iv}} - T_{\text{in}}) - \frac{1}{R_4}(T_{\text{iv}} - T_{\text{Hin}}) - \frac{1}{R_6}(T_{\text{iv}} - T_{\text{comb}}) \tag{8}$$

$$C_{\text{ev}}\frac{dT_{\text{ev}}}{dt} = -\frac{1}{R_8}(T_{\text{ev}} - T_{\text{comb}}) - \frac{1}{R_{11}}(T_{\text{ev}} - T_{\text{ex}}) - \frac{1}{R_{12}}(T_{\text{ev}} - T_{\text{Hex}}) \tag{9}$$

The expressions that describe the exchange of energy for the piston and lubricating oil are

$$C_{\text{pist}}\frac{dT_{\text{pist}}}{dt} = -\frac{1}{R_{19}}(T_{\text{pist}} - T_{\text{comb}}) - \frac{1}{R_{20}}(T_{\text{pist}} - T_{\text{oil}}) - \frac{1}{R_{23}}(T_{\text{pist}} - T_{c2}) - \frac{1}{R_{24}}(T_{\text{pist}} - T_{c1}) \tag{10}$$

$$C_{\text{oil}}\frac{dT_{\text{oil}}}{dt} = -\frac{1}{R_{20}}(T_{\text{oil}} - T_{\text{pist}}) - \frac{1}{R_{25}}(T_{\text{oil}} - T_{c1}) - \frac{1}{R_{31}}(T_{\text{oil}} - T_\infty) \tag{11}$$

Similar to the engine cylinder head, the cylinder wall is also characterized by three nodes, that is, C_{c1}, C_{c2}, and C_{c3}, that represent the lower, middle, and upper portions of the cylinder side wall, respectively. Again, the selection of these nodes corresponds to the physical travel of the piston. For instance, node C_{c1} is not exposed to the combustion gases while it is exposed to the lubricating oil. The differential equations may be written as

$$C_{c1}\frac{dT_{c1}}{dt} = -\frac{1}{R_{24}}(T_{c1} - T_{pist}) - \frac{1}{R_{25}}(T_{c1} - T_{oil}) - \frac{1}{R_{27}}(T_{c1} - T_{c2}) - \frac{1}{R_{30}}(T_{c1} - T_{\infty}) \quad (12)$$

$$C_{c2}\frac{dT_{c2}}{dt} = -\frac{1}{R_{22}}(T_{c2} - T_{comb}) - \frac{1}{R_{23}}(T_{c2} - T_{pist}) - \frac{1}{R_{26}}(T_{c2} - T_{c3}) - \frac{1}{R_{27}}(T_{c2} - T_{c1}) - \frac{1}{R_{29}}(T_{c2} - T_{\infty}) \quad (13)$$

$$C_{c3}\frac{dT_{c3}}{dt} = -\frac{1}{R_{17}}(T_{c3} - T_{Hm}) - \frac{1}{R_{21}}(T_{c3} - T_{comb}) - \frac{1}{R_{26}}(T_{c3} - T_{c2}) - \frac{1}{R_{28}}(T_{c3} - T_{\infty}) \quad (14)$$

Finally, the effect of the engine components on the surrounding air temperature becomes

$$C_{\infty}\frac{dT_{\infty}}{dt} = -\frac{1}{R_1}(T_{\infty} - T_{in}) - \frac{1}{R_9}(T_{\infty} - T_{ex}) - \frac{1}{R_{14}}(T_{\infty} - T_{Hin}) - \frac{1}{R_{15}}(T_{\infty} - T_{Hm}) - \frac{1}{R_{16}}(T_{\infty} - T_{Hex}) - \frac{1}{R_{28}}(T_{\infty} - T_{c3}) - \frac{1}{R_{29}}(T_{\infty} - T_{c2}) - \frac{1}{R_{30}}(T_{\infty} - T_{c1}) - \frac{1}{R_{31}}(T_{\infty} - T_{oil}) \quad (15)$$

The resistive elements R_1–R_{31} must now be considered using the definitions of Table 1. The following eight resistances describe the pure convection that occurs between the various engine nodes:

$$R_1 = 1/C_{p\infty}\dot{m}_{A/F}, \quad R_2 = 1/h_{in}A_{Hin}, \quad R_3 = 1/h_{in}A_{ivf}$$
$$R_9 = 1/C_{p\,comb}\dot{m}_{A/F}, \quad R_{10} = 1/h_{ex}A_{Hex}, \quad R_{11} = 1/h_{ex}A_{evf}$$
$$R_{25} = 1/h_{oil}A_{c1e}, \quad R_{31} = 1/h_{op}A_{oil} \quad (16)$$

Similarly, the thermal conduction resistance between the engine nodes may be stated as

$$R_5 = \frac{L_{R5}}{k_{head}A_{R5}}, \quad R_{13} = \frac{L_{R13}}{k_{head}A_{R13}}, \quad R_{17} = \frac{L_{gasket}}{k_{gasket}A_{gasket}}$$
$$R_{26} = \frac{L_{R26}}{k_{cyl}A_{R26}}, \quad R_{27} = \frac{L_{R27}}{k_{cyl}A_{R27}} \quad (17)$$

To describe the contact resistance between two periodically contacting surfaces, constant values have been used, in this instance, the heat transfer between the valves and the valve seats, that is, R_4 and R_{12}, and the thermal flow of energy from the hot combustion gases to the exhaust node, that is, R_{18}. These resistive terms may be expressed mathematically as

$$R_4 = \left[\left(\frac{L_{vs}}{K_{valve}A_{vs}} + \frac{L_{vg}}{K_{vg}A_{vg}} + \frac{L_{hv}}{K_{head}A_{hv}}\right)^{-1} + (R_{contact})^{-1}\right]^{-1} \quad (18a)$$

$$R_{12} = \left[\left(\frac{L_{vs}}{K_{valve}A_{vs}} + \frac{L_{vg}}{K_{vg}A_{vg}} + \frac{L_{hv}}{K_{head}A_{hv}}\right)^{-1} + (R_{contact})^{-1}\right]^{-1} \quad (18b)$$

$$R_{18} = \left(\frac{1}{\dot{m}C_p}\right)f(\theta) \quad (18c)$$

The individual resistances between the piston and select cylinder wall sections are

$$R_{23} = \left\{\left(\frac{3}{R_r}\right)^{-1} + \left[\frac{T_{pist} - T_{c2}}{A_{pistw}\sigma\varepsilon_{pist}\left(T_{pist}^4 - T_{c2}^4\right)}\right]^{-1}\right\}^{-1} \quad (19a)$$

$$R_{24} = \left\{\left(\frac{3}{R_r}\right)^{-1} + \left[\frac{T_{pist} - T_{c1}}{A_{pistw}\sigma\varepsilon_{pist}\left(T_{pist}^4 - T_{c1}^4\right)}\right]^{-1}\right\}^{-1} \quad (19b)$$

Note that these expressions are combinations of the radiation and conductive resistance across the piston ring and oil film, respectively. Last, the remaining 13 resistances are a summation of parallel conduction and radiation thermal paths that exist within the engine:

$$R_6 = \left\{\left(\frac{1}{h_{comb}A_{iv}}\right)^{-1} + \left[\frac{T_{iv} - T_{comb}}{A_{iv}\sigma\varepsilon_{comb}\left(T_{iv}^4 - T_{comb}^4\right)}\right]^{-1}\right\}^{-1} \quad (20a)$$

$$R_7 = \left\{\left(\frac{1}{h_{comb}A_{Hm}}\right)^{-1} + \left[\frac{T_{Hm} - T_{comb}}{A_{Hm}\sigma\varepsilon_{comb}\left(T_{Hm}^4 - T_{comb}^4\right)}\right]^{-1}\right\}^{-1} \quad (20b)$$

$$R_8 = \left\{\left(\frac{1}{h_{comb}A_{ev}}\right)^{-1} + \left[\frac{T_{ev} - T_{comb}}{A_{ev}\sigma\varepsilon_{comb}\left(T_{ev}^4 - T_{comb}^4\right)}\right]^{-1}\right\}^{-1} \quad (20c)$$

$$R_{14} = \left(\left[\frac{1}{h_{\infty}(A_{vc}/3)} + \frac{1}{h_{tube}(A_{tube}/3)} + \frac{1}{h_{hf}(A_{hf}/3)}\right]^{-1} + \left\{\frac{T_{Hin} - T_{\infty}}{[(A_{vc} + A_{tube} + A_{hf})/3]\sigma\varepsilon_{head}\left(T_{Hin}^4 - T_{\infty}^4\right)}\right\}^{-1}\right)^{-1} \quad (20d)$$

$$R_{15} = \left(\left[\frac{1}{h_{\infty}(A_{vc}/3)} + \frac{1}{h_{tube}(A_{tube}/3)} + \frac{1}{h_{hf}(A_{hf}/3)}\right]^{-1} + \left\{\frac{T_{Hm} - T_{\infty}}{[(A_{vc} + A_{tube} + A_{hf})/3]\sigma\varepsilon_{head}\left(T_{Hm}^4 - T_{\infty}^4\right)}\right\}^{-1}\right)^{-1} \quad (20e)$$

$$R_{16} = \left(\left[\frac{1}{h_{\infty}(A_{vc}/3)} + \frac{1}{h_{tube}(A_{tube}/3)} + \frac{1}{h_{hf}(A_{hf}/3)}\right]^{-1} + \left\{\frac{T_{Hex} - T_{\infty}}{[(A_{vc} + A_{tube} + A_{hf})/3]\sigma\varepsilon_{head}\left(T_{Hex}^4 - T_{\infty}^4\right)}\right\}^{-1}\right)^{-1} \quad (20f)$$

$$R_{19} = \left\{\left[\frac{1}{h_{comb}A_{pistc}}\right]^{-1} + \left[\frac{T_{pist} - T_{comb}}{A_{pistc}\sigma\varepsilon_{comb}\left(T_{pist}^4 - T_{comb}^4\right)}\right]^{-1}\right\}^{-1} \quad (20g)$$

$$R_{20} = \left\{\left(\frac{1}{h_{oil}A_{pisto}}\right)^{-1} + \left[\frac{T_{pist} - T_{oil}}{A_{pisto}\sigma\varepsilon_{comb}\left(T_{pist}^4 - T_{oil}^4\right)}\right]^{-1}\right\}^{-1} \quad (20h)$$

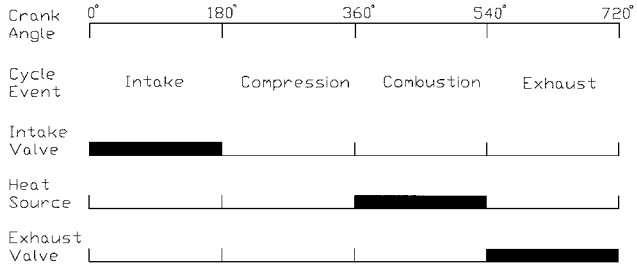

Fig. 4 Heat source and valve motion indexed to the crank angle.

$$R_{21} = \left\{ \left(\frac{1}{h_{\text{comb}} A_{c3}} \right)^{-1} + \left[\frac{T_{c3} - T_{\text{comb}}}{A_{c3} \sigma \varepsilon_{\text{comb}} \left(T_{c3}^4 - T_{\text{comb}}^4 \right)} \right]^{-1} \right\}^{-1} \tag{20i}$$

$$R_{22} = \left\{ \left(\frac{1}{h_{\text{comb}} A_{c2}} \right)^{-1} + \left[\frac{T_{c2} - T_{\text{comb}}}{A_{c2} \sigma \varepsilon_{\text{comb}} \left(T_{c2}^4 - T_{\text{comb}}^4 \right)} \right]^{-1} \right\}^{-1} \tag{20j}$$

$$R_{28} = \left\{ \left(\frac{1}{h_{\infty} A_{c3e}} \right)^{-1} + \left[\frac{T_{c3} - T_{\infty}}{A_{c3e} \sigma \varepsilon_{\text{cyl}} \left(T_{c3}^4 - T_{\infty}^4 \right)} \right]^{-1} \right\}^{-1} \tag{20k}$$

$$R_{29} = \left\{ \left(\frac{1}{h_{\infty} A_{c2e}} \right)^{-1} + \left[\frac{T_{c2} - T_{\infty}}{A_{c2e} \sigma \varepsilon_{\text{cyl}} \left(T_{c2}^4 - T_{\infty}^4 \right)} \right]^{-1} \right\}^{-1} \tag{20l}$$

$$R_{30} = \left\{ \left(\frac{1}{h_{\infty} A_{c1e}} \right)^{-1} + \left[\frac{T_{c1} - T_{\infty}}{A_{c1e} \sigma \varepsilon_{\text{cyl}} \left(T_{c1}^4 - T_{\infty}^4 \right)} \right]^{-1} \right\}^{-1} \tag{20m}$$

The combustion gases convection coefficient are calculated as $h_{\text{comb}} = 10.4(B^{-1} k_{\text{gas}})(Re_{\text{comb}})^{0.75}$, where $Re_{\text{comb}} = \dot{m}_{\text{gas}} B / A_p \mu_{\text{gas}}$ and $\dot{m}_{\text{gas}} = \dot{m}_f + \dot{m}_a$.

The cyclic nature of the internal combustion engine process means that the heat created is not constant throughout the 720-deg crank angle degrees of one cycle. Specifically, each spark plug is periodically fired once every two revolutions of the crankshaft during its respective power portion of the cycle. For the hypothetical case shown in Fig. 4, the combustion event occurs between 180 and 360 deg. The intake and exhaust valve openings are also shown; they regulate the flow of gases into/out of the cylinder. These three cyclic events must be represented in the dynamic simulation to describe fully the thermal behavior of the engine. If the engine is operating at a speed of $N = 2000$ rpm, then this corresponds to a combustion event between $t = 0.015$ and 0.030 s for a $t = 0.06$ s cycle.

The thermal differential equations (1–20) may be represented in the state-space form of

$$\dot{x} = A(\boldsymbol{x}, \boldsymbol{u}, \theta, \phi)\boldsymbol{x} + B(\theta, \phi)\boldsymbol{u} \tag{21a}$$

$$\boldsymbol{y} = C\boldsymbol{x} \tag{21b}$$

where $\boldsymbol{x} \in R^{14 \times 1}$, $\boldsymbol{y} \in R^{14 \times 1}$, $\boldsymbol{u} \in R^{1 \times 1}$, and ϕ denotes model parameters. The state vector for the thermal model is $\boldsymbol{x} = [T_{\text{comb}}, T_{\text{in}}, T_{\text{Hin}}, T_{\text{Hm}}, T_{\text{Hex}}, T_{\text{ex}}, T_{\text{iv}}, T_{\text{ev}}, T_{\text{pist}}, T_{c1}, T_{c2}, T_{c3}, T_{\text{oil}}, T_{\infty}]^T$, and the output matrix C is the identity matrix.

IV. Experimental and Numerical Results

The target application is a four-stroke air-cooled internal combustion spark ignition utility engine. These portable engines are used worldwide for transportation, power generation, and fluid movement systems. Recent hybrid electric vehicles, for example, parallel configuration with electric motor and gasoline engine, have focused on smaller displacement engines to augment the electric drive motor to satisfy horsepower requirements (e.g., Smith and Franchek[28]). To validate the mathematical model's estimation of component temperatures for a typical operating cycle, representative experimental and numerical results will be presented and discussed.

The experimental activities have been conducted in the Automotive Research Laboratory. A new overhead valve, 14.9-kW Briggs and Stratton (Model 351447) engine was attached to an International Dynamometer Corp. (Model 500) power absorption dynamometer and instrumented with a variety of sensors. The cylinder head, cylinder wall, and oil reservoir temperatures were measured with T-type "special limit of error" thermocouples (± 0.5°C), and the exhaust gas temperature was measured with K-type special limit of error thermocouples (± 1.0°C). The cylinder head thermocouple was mounted on the rear side, that is, output shaft, of the cylinder between cooling fins 1 and 2 on the head along the bore's centerline. The cylinder wall thermocouple was placed on the same centerline in a recess next to the sixth fin on the engine block. The exhaust thermocouple was inserted into the exhaust stream at the beginning of an exhaust manifold run, and the oil reservoir probe was attached to the dip stick and inserted into the oil reservoir with the tip fully immersed in the oil and not contacting the stick. These signals were logged using an Omega thermocouple thermometer. Other engine instrumentation included a multipurpose data acquisition unit to provide engine speed and dynamometer readings for the applied load. For this engine, the maximum cylinder head, oil, and fuel temperatures were factory rated at 277, 154, and 54.4°C, respectively. Data were logged at an initial time interval of 30 s for the first 12 min and then every 60 s as the engine approached steady-state operating conditions. After 25 min, the engine was shut off, and temperatures were logged for another 25 min during the cool-down period. For this study, a series of six tests were conducted each at no-load and load for speeds ranging $1600 \leq N \leq 2600$ rpm in $\Delta N = 200$ rpm increments. The experimental results are presented in Fig. 5 for the engine operating at 2000 rpm with 19.4 N·m, that is, 27.3% of full, load. As shown, the exhaust gases have the highest steady-state temperature followed by the cylinder head, cylinder wall, and oil reservoir.

A MATLAB®/Simulink™ simulation was created for the multinode thermal model. A Dormand–Prince integration scheme was selected with an integration time step of $\Delta t = 0.001$ s and a simulation end time of $t_f = 50$ min. The engine's operating speed was selected as $N = 2000$ rpm to allow computation of the crank shaft angle. The initial conditions for the differential equations were selected at the ambient temperature of 20.8°C. To conduct the numerical simulations, a number of system parameters had to be predetermined such as the heat transfer coefficient corresponding to the combustion gases, for example, approximate value of 300 W/m^2·K, engine areas, for example, cylinder head, piston, cylinder wall, etc., and

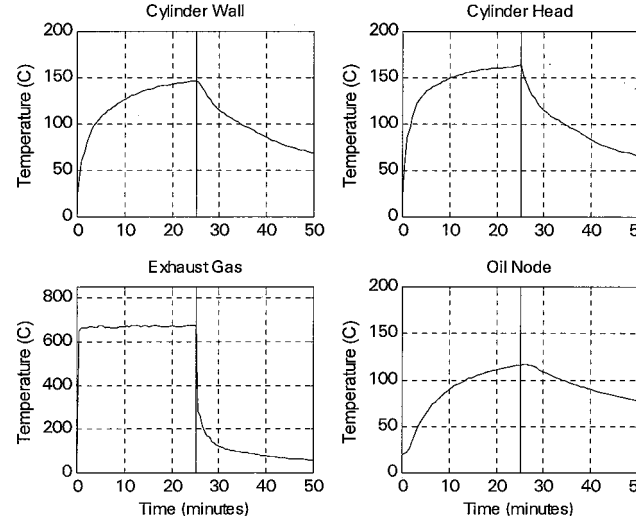

Fig. 5 Experimental test results for an air-cooled engine operating with load at 2000 rpm and ambient air temperature of 20.8°C.

Table 2 Summary of thermal model parameters

Symbol	Value	Unit	Symbol	Value	Unit
AFR	14.70	——	C_{pist}	1.3651e−02	J/K
A_{c1}	2.8274e−02	m^2	C_{∞}	1.007e−08	J/K
A_{c2}	2.8274e−02	m^2	$c_{p_{\text{comb}}}$	1.918e−03	J/kg · K
A_{c3}	2.8274e−02	m^2	$c_{p_{\infty}}$	1.007e−03	J/kg · K
A_{c1e}	1.037e−02	m^2	h_{comb}	500.0	W/m^2 · K
A_{c2e}	2.367e−02	m^2	h_{cyl}	110.44	W/m^2 · K
A_{c3e}	2.6360e−02	m^2	h_{ex}	3000	W/m^2 · K
A_{c1o}	3.9540e−02	m^2	h_{hf}	107.72	W/m^2 · K
A_{ev}	4.5239e−04	m^2	h_{in}	200	W/m^2 · K
$A_{\text{ev-con}}$	1.400e−04	m^2	h_{oil}	240.0	W/m^2 · K
A_{evf}	6.7858e−04	m^2	h_{op}	94.5	W/m^2 · K
A_{gasket}	4.00e−03	m^2	h_{tube}	105.75	W/m^2 · K
A_{hf}	5.4300e−02	m^2	h_{∞}	50	W/m^2 · K
A_{hv}	1.3195e−03	m^2	K	0.9	——
A_{Hex}	3.2987e−03	m^2	k_{cyl}	180	W/m · K
A_{Hin}	3.6128e−03	m^2	k_{gas}	5.29e−02	W/m · K
A_{Hm}	3.0882e−03	m^2	k_{gasket}	180	W/m · K
A_{iv}	5.3093e−04	m^2	k_{head}	180	W/m · K
A_{ivf}	7.9639e−04	m^2	k_{valve}	14.5	W/m · K
A_{oil}	3.20e−02	m^2	k_{vg}	14.5	W/m · K
A_{pistc}	4.0712e−03	m^2	L_{gasket}	1.50e−03	m
A_{pisto}	1.0179e−02	m^2	L_{hv}	5.00e−03	m
A_{pistw}	1.2441e−02	m^2	L_{vg}	2.00e−03	m
A_{R_5}	7.00e−03	m^2	L_{vs}	1.00e−02	m
$A_{R_{13}}$	7.00e−03	m^2	L_{R_5}	3.50e−02	m
$A_{R_{26}}$	2.0106e−03	m^2	$L_{R_{13}}$	3.50e−02	m
$A_{R_{27}}$	2.0106e−03	m^2	$L_{R_{26}}$	4.1667e−02	m
A_{tube}	1.8500e−02	m^2	$L_{R_{27}}$	4.1667e−02	m
A_{vc}	1.5600e−02	m^2	$\dot{m}_a$	2.4667e−02	kg/s
A_{vg}	6.5973e−04	m^2	$\dot{m}_f$	1.6780e−03	kg/s
A_{vs}	3.8485e−05	m^2	$\dot{m}_{\text{A/F}}$	2.6345e−02	kg/s
C_{c1}	3.2324e−02	J/K	N	2.00e−03	rpm
C_{c2}	3.2324e−02	J/K	Q_{comb}	6.6449e−04	W
C_{comb}	3.032	J/K	Q_{low}	4.4e−07	J/kg
C_{c3}	3.2324e−02	J/K	R_r	4.6672	K/W
C_{ev}	1.3411e−01	J/K	t_f	50	min
C_{ex}	1.655	J/K	Δt	1.00e−03	s
C_{Hex}	4.5009e−02	J/K	μ_{gas}	3.274e−05	m^2/s
C_{Hin}	4.5009e−02	J/K	σ	5.670e−08	W/m^2 · K^4
C_{Hm}	4.5009e−02	J/K	ε_{cyl}	0.64	——
C_{in}	1.655	J/K	$\varepsilon_{\text{comb}}$	0.10	——
C_{iv}	1.4496e−01	J/K	$\varepsilon_{\text{head}}$	0.60	——
C_{oil}	3.3348e−03	J/K	$\varepsilon_{\text{piston}}$	0.61	——

various thermal conductivities including the periodic contact resistance at the valve–valve seat interface. The thermal model parameters are listed in Table 2. These values were analytically estimated and validated through experimental testing with a 19.4 N · m load. Representative numerical results are presented in Fig. 6 for periodic combustion and intake/exhaust valve events. In Fig. 6, the cylinder wall, cylinder head, valves, piston, oil, inlet, exhaust, and combustion temperatures (°C) are displayed vs time (minutes). The AFR, or $\dot{m}_{\text{fuel}}$, was adjusted in Eq. (2) to reflect the dynamometer load applied to the engine. A limitation of this proposed methodology is the required knowledge of the ECU-based fueling map and assumption of stoichiometric operating conditions. The numerical results agree favorably with a 1.61% error for the middle cylinder head temperature T_{Hm}, an error of 5.73% for the middle cylinder wall temperature T_{c2}, an error of 6.65% for the oil temperature T_{oil}, and a 3.56% error for the exhaust temperature, T_{ex}. Overall, these numerical results demonstrate the feasibility of applying a lumped-parameter RC network strategy to estimate the in-cylinder temperatures. Attention will now focus on calculating the periodic contact resistance across the exhaust valve's thermal junction.

V. Investigation of Periodic Contact Resistance

In many practical engineering problems, the heat transfer between periodic surfaces often results in an imperfect thermal contact. Mechanical components in rotational devices, such as internal combustion engines, have periodic heat transfer processes occurring across numerous contact surfaces. One fascinating example involves

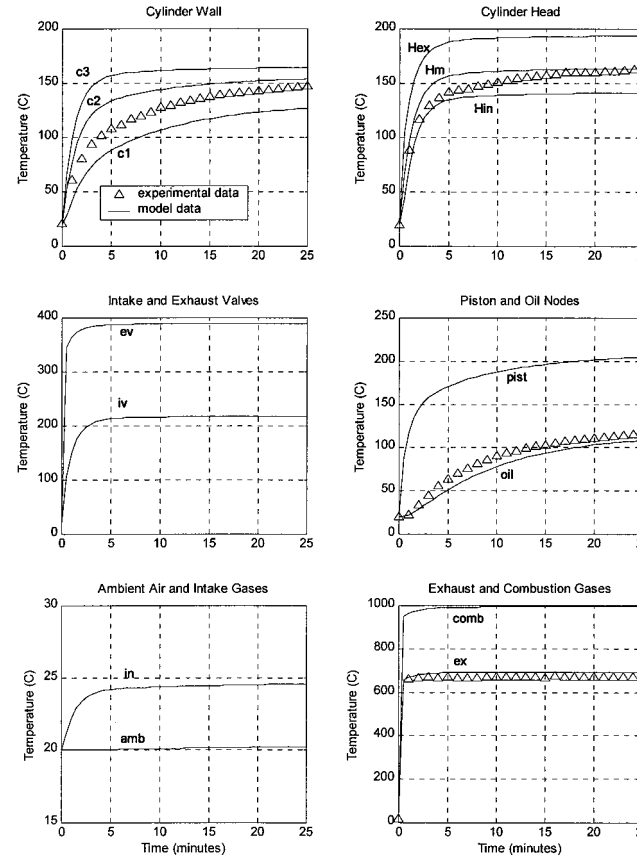

Fig. 6 Predicted and experimental temperatures of an air-cooled engine operating with load at 2000 rpm and ambient air temperature of 20.8°C.

the transfer of thermal energy across the beveled area of an exhaust valve and the stainless steel seat insert located within some aluminum engine blocks. Substantial analytical and experimental investigations have been conducted in the past to predict and measure periodic thermal contact resistance. For instance, analytical computations of the temperature distribution in periodically contacting regions when the contact resistance was known has been extensively studied.[9,10,29] Finite difference equations were employed for conditions of perfect contact whereas the imperfect thermal contact problem was solved with an integral transform technique.

The experimental efforts, involving periodically contacting surfaces, specifically focused on measuring a constant contact resistance during the contact mode of a periodic contact/noncontact operation.[12,13,30] The experimental apparatus involved two one-dimensional rods with each of the noncontacting ends held at a closely controlled fixed temperature. The radial heat transfer component was negligible because insulation was placed around the rods so that the heat transfer was effectively one dimensional. The contact resistance was estimated from surface temperature and heat flux values calculated using a linear, or quadratic, extrapolation method. The goal of the present investigation was to determine the periodic contact resistance between the exhaust valve and cylinder head from experimentally gathered temperatures. Thermocouples were strategically located on an air-cooled internal combustion engine such that the predicted component temperatures could be matched to the experimentally gathered data. This procedure allowed the determination of the nodal temperatures between the exhaust valve and cylinder head that in turn allowed the computation of the thermal contact resistance at the beveled valve-cylinder head interface region.

The contact resistance between the valve and the cylinder head was modeled for constant steady-state conditions. The heat flowing to the exhaust valve, Q_{in}, can be expressed as

$$Q_{\text{in}} = (1/R_8)(T_{\text{comb}} - T_{\text{ev}}) \tag{22}$$

Heisler[31] and Yang et al.[32] state that, for steady-state and closed valve conditions, approximately 76% of the heat in the valve stem transfers through the valve seat, that is, Q_{contact}, whereas the remaining 24% travels through the valve stem, that is, Q_{vg}, or

$$Q_{\text{out}} = Q_{\text{contact}} + Q_{\text{vg}} = 0.76Q_{\text{in}} + 0.24Q_{\text{in}} \tag{23}$$

The 76/24% ratio split in heat transfer rate was taken from liquid-cooled engine data with the assumptions of solid valve stem, similar valve–valve seat configuration, and standard production engine (two cylinders). Except for the liquid-cooled engine condition, all others were implemented into our experimental investigation. Although the use of this ratio will introduce an error into our analysis, presently very little information exists for air-cooled engines. However, the error introduced should be small because the use of heat transfer fins, which are an integral part of the engine housing design, should cause the paths to be similar to liquid-cooled engines. The detractors from Heisler's investigation[31] are the engine speed (3600 vs 2000 rpm) and AFR (13.5 vs 14.7) when compared to our study. These parameters should not significantly affect the outcome of our results.

The heat transferred Q between two nodes of the lumped capacitance model was calculated as $Q = R^{-1}(\Delta T)$, where ΔT is the temperature differential. Thus, the contact resistance for the valve, R_{contact}, may be initially expressed as

$$R_{\text{contact}} = (1/Q_{\text{contact}})(T_{\text{Hex}} - T_{\text{ev}}) = (1/0.76Q_{\text{in}})(T_{\text{Hex}} - T_{\text{ev}}) \tag{24}$$

Finally, substituting Eq. (22) into Eq. (24) yields the periodic contact resistance

$$R_{\text{contact}} = \frac{R_8}{0.76}\frac{(T_{\text{Hex}} - T_{\text{ev}})}{(T_{\text{ev}} - T_{\text{comb}})} \tag{25}$$

Note that the temperatures of the cylinder head, T_{Hex}, exhaust valve, T_{ev}, and combustion gases, T_{comb}, are each dependent on time and the engine speed; however, for this investigation, steady-state temperatures were employed for the calculation of periodic contact resistance. In Fig. 7, the thermal contact resistance is displayed for four different engine speeds, that is, $N = 1500$, 2000, 2400, and 3000 rpm, as a function of time. The numerically estimated resistance values begin at $t = 0.40$ s to account for the small combustion temperature lag; before this time instance, the values have been extrapolated. As expected, the contact resistance magnitudes decrease as the engine temperatures rise based on the cylinder–head transient thermal response. Furthermore, the engine speed influences the contact resistance through the exhaust valve opening/closing frequency and nodal temperature changes. The steady-state magnitudes for the periodic contact resistance are in the range $1.75 \leq R_{\text{contact}} \leq 1.85$ (K/W) or $3.86 \times 10^3 \leq h_{\text{contact}} \leq 4.08 \times 10^3$ (W/m$^2 \cdot$K).

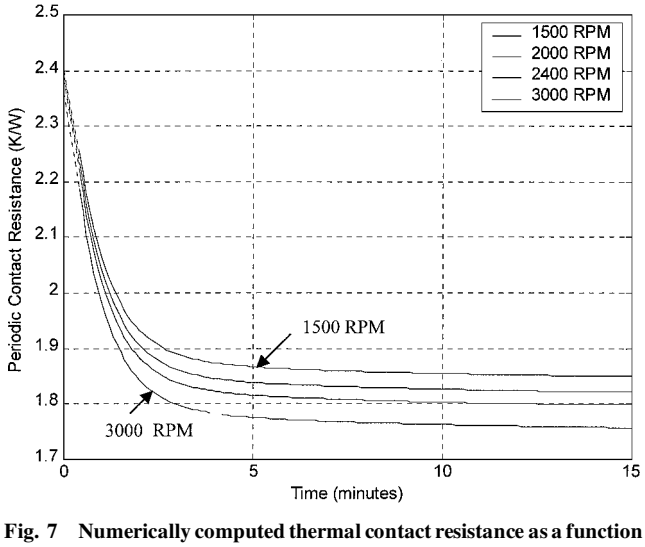

Fig. 7 Numerically computed thermal contact resistance as a function of time for four engine speeds.

For comparison purposes, Moses and Dodd[33] studied periodic contact across aluminum/stainless-steel surfaces at a contact pressure of 85 kPa and mean temperature of 48.5°C. They reported a quasi-steady-state thermal conductance value equal to 1.50×10^3 (W/m$^2 \cdot$K). The difference between the present values and theirs may be primarily attributed to several application specific factors. First, the mean interface temperature of the exhaust valve and cylinder head for this investigation was computed to be 290°C. Thus, a larger convection coefficient may be realized due to the higher interface mean temperatures. Second, the applied mean pressure due to cyclic in-cylinder gases[34] and the exhaust valve spring, acting at the valve's contact interface, is approximately 3.25×10^3 kPa. The larger applied loading provides an opportunity for greater asperity deformation, thus greater contact area for heat transfer. Next, the contact/separation interval is a function of engine speed and ranges $0.04 \leq t \leq 0.08$ s in contrast to the $15 \leq t \leq 120$ s interval of Moses and Dodd.[33] Finally, a heat transfer rate of 76% (24%) through the valve seat (stem) has been applied to compute the contact resistance based on Heisler.[31] However, these distribution values are certainly application dependent to some extent and ultimately impact the computed periodic contact magnitudes.

The experimental study and analysis of valve-seat periodic contact for an internal combustion engine conducted by Couedel et al.[14] gave an empirical relationship between frequency ν and overall mean contact resistance $\bar{R}_c$ as

$$\bar{R}_c = 21.4/(1 + \nu/12.7) \tag{26}$$

If one applies their expression to conditions for this investigation, for example, 1500–3000 rpm, then the range of the computed magnitude for the periodic contact resistance lies between 0.83 and 1.60 (K/W). The relative error for these computed values is 5.8%, which is the stated error mentioned by the authors. If one considers that the material set for the valve–valve seat contact may not be identical to the experimental engine employed presently, the agreement is quite good.

The completion of an uncertainty analysis for this study embodied the identification and quantification of errors. In this case, one error source was considered the most decisive, that is, simulation errors associated with the mathematical model, to gaining insight into the uncertainty associated with the periodic contact resistance calculations. The mathematical model requires a database of over 80 parameters ranging from engine nodal areas to convection heat transfer coefficients to gasket thickness, as listed in Table 2. The basis for these parameters was either laboratory measurements or published technical information. It has been difficult to quantify the uncertainty of each individual parameter; therefore, a concerted emphasis was placed on the highest source of computational uncertainty, that is, the convective coefficients employed for the model predictions. These parameters consisted of the exhaust gases h_{ex}, incoming fuel mixture h_{in}, piston to oil h_{oil}, ambient air and oil pan h_{op}, and ambient air through head tubes h_{tube}.

The simulation model, described by Eqs. (1–20), was validated using engine test data (Fig. 5). As reported, the percent difference between the model estimated and experimentally measured temperatures ranged from 1.61 to 6.65% at the four temperature locations. The periodic contact resistance was calculated using Eqs. (22–25), which depends on the estimated temperatures, model database, and the heat transfer paths for the exhaust valve at the valve seat and valve stem. Therefore, a realistic estimate of the periodic contact resistance uncertainty was computed with respect to the simulation propagation errors using the rss method:

$$w_{\text{pcr}} = \pm\sqrt{e_{R_8}^2 + e_{T_{\text{Hex}}}^2 + e_{T_{\text{ev}}}^2 + e_{T_{\text{comb}}}^2} \tag{27}$$

In other words, the elemental errors were computed using an rss method with an underlying assumption that the errors encountered tend to follow a Gaussian distribution. Therefore, the rss estimate of all contributing errors provides a probable measure of the error

of the periodic contact resistance. The uncertainty of type T special limit of error thermocouples used to measure the head exhaust section T_{Hex} and estimate the exhaust valve T_{ev} temperatures is 0.4%. The uncertainty with respect to the use of type K special limit of error, which was employed to measure the combustion temperature T_{comb} via the exhaust manifold stream is also 0.4%. The uncertainty associated with R_8 is similar to the uncertainty for the periodic contact resistance; however, a few additional parameters must be included, such as the uncertainty in the surface area of contact A_{ev} and emissivity $\varepsilon_{\text{comb}}$, which are equal to 4 and 10%, respectively. The rss method may also be employed to R_8:

$$w_{R_8} = \pm\sqrt{e_{h_{\text{comb}}}^2 + e_{A_{\text{ev}}}^2 + e_{T_{\text{ev}}}^2 + e_{T_{\text{comb}}}^2 + e_{\varepsilon_{\text{comb}}}^2} \qquad (28)$$

With these parameters in mind, the uncertainty in R_8 was determined to be 22.7% . The uncertainty in the periodic contact resistance was computed as 23%. Although this may seem a bit high, the largest contributorto the uncertainty lies in the convective coefficient h_{comb}, which has been estimated to be roughly 20% (Ref. 26).

VI. Conclusions

In this paper, the thermal behavior of engine cylinder components has been investigated. To estimate the temperature of exhaust valves, a 14 node nonlinear thermal model was derived using both analytical and empirical relationships. The 14 nodes include the engine head, cylinder wall, intake and exhaust valves, piston, oil, surrounding air, and gases in the inlet, exhaust, and undergoing combustion. Representative experimental and numerical results were presented and discussed to demonstrate the validity of the lumped parameter resistance–capacitance network modeling technique. A literature survey of thermal periodic contact was presented with extension to exhaust valves in internal combustion engines. The periodic contact resistance between the exhaust valve and cylinder head was investigated for various engine operating conditions. This thermal model will be the cornerstone of air and coolant flow regulation strategies in spark ignition and compression engines to enhance the thermal management system's functionality.

Acknowledgment

The authors wish to thank the anonymous reviewers for providing insightful comments.

References

[1]Kelly, D., and Shannon, G. F., "Automotive Electronics and Engine Management Systems—A Review," *Australian Journal of Electrical and Electronics Engineering*, Vol. 10, No. 4, 1990, pp. 286–297.

[2]Heywood, J. B., *Internal Combustion Engine Fundamentals*, McGraw–Hill, New York, 1988.

[3]Visnic, B., "Thermostat, Thy Days are Numbered," *Wards Auto World*, Vol. 37, No. 6, 2001, pp. 53, 54.

[4]Wagner, J., Paradis, I., Marotta, E., and Dawson, D., "Enhanced Automotive Engine Cooling Systems—A Mechatronics Approach," *International Journal of Vehicle Design* (to be published).

[5]Nichols, R. W., Ramsey, B. W., Marotta, E. E., and Wagner, J. R., "Thermal Periodic Contact of Exhaust Valves in Spark Ignition Internal Combustion Engines for Improved Control Performance," AIAA Paper 2000-0878, Jan. 2000.

[6]Reed, J. R., and Mullineux, G., "Quasi-Steady State Solution of Periodically Varying Phenomena," *International Journal of Heat and Mass Transfer*, Vol. 16, 1973, pp. 2007–2012.

[7]Howard, J. R., and Sutton, A. E., "The Effect of Thermal Contact Resistance on Heat Transfer between Periodically Contacting Surfaces," *Journal of Heat Transfer*, Vol. 95C, 1973, pp. 411, 412.

[8]Mikhailov, M. D., "Quasi-Steady State Temperature Distribution in Finite Regions with Periodically Varying Boundary Conditions," *International Journal of Heat and Mass Transfer*, Vol. 17, 1974, pp. 1475–1478.

[9]Vick, B., and Ozisik, M. N., "Quasi-Steady State Temperature Distribution in Periodically Contacting Finite Regions," *Journal of Heat Transfer*, Vol. 103, 1981, pp. 739–744.

[10]Flach, G. P., and Ozisik, M. N., "Inverse Heat Conduction Problem of Periodically Contacting Surfaces," *Journal of Heat Transfer*, Vol. 110, 1988, pp. 821–829.

[11]Huang, C. H., and Ju, T. M., "Inverse Problem of Determining the Periodic Thermal Contact Conductance Between Exhaust Valve and Seat in an Internal Combustion Engine," National Heat Transfer Conf., 1993.

[12]Howard, J. R., "An Experimental Study of Heat Transfer Through Periodically Contacting Surfaces," *International Journal of Heat and Mass Transfer*, Vol. 19, 1976, pp. 367–372.

[13]Moses, W. M., and Johnson, R. R., "Experimental Study of the Transient Heat Transfer Across Periodically Contacting Surfaces," *Journal of Thermophysics and Heat Transfer*, Vol. 2, No. 1, 1988, pp. 37–42.

[14]Couedel, D., Danes, F., and Bardon, J. P., "Experimental Study and Analysis of Heat Transfer in a Valve-Seat Periodic Contact in an Internal Combustion Engine," American Society of Mechanical Engineers Meeting, 1991.

[15]Fenech, H., and Rosenhow, W. M., "Prediction of Thermal Contact Conductance of Metallic Surfaces in Contact," *Journal of Heat Transfer*, Vol. 85, 1963, pp. 15–42.

[16]Fenech, H., Henry, J. J., and Rosenhow, W. M., "Thermal Contact Conductance," *Developments in Heat Transfer*, Edward Arnold, London, 1964, Chap. 13.

[17]Fletcher, L. S., and Gyorog, D. A., "Heat Transfer between Surfaces in Contact: An Analytically and Experimental Study of Thermal Contact Resistance of Metallic Surfaces," Dept. of Mechanical Engineering, Rept. ME-TR-033-4, Arizona State Univ., Tempe, AZ, 1971; also NASA CR-114373, 1971.

[18]Cooper, M., Mikic, B. B., and Yovanovich, M. M., "Thermal Contact Conductance," *International Journal of Heat and Mass Transfer*, Vol. 12, 1969, pp. 279–300.

[19]Thomas, T. R., and Probert, S. D., "Correlations for Thermal Contact Conductance in vacuo," *Journal of Heat Transfer*, Vol. 94C, 1972, pp. 276–280.

[20]Marotta, E. E., Fletcher, L. S., Aikawa, T., Maki, K., and Aoki, Y., "The Thermal Contact Conductance of Sintered Copper Coatings on Sintered Ferro-Alloy at High Contact Temperatures and Pressures," *Journal of Heat Transfer*, Vol. 121, No. 1, 1999, pp. 177–182.

[21]Shayler, P. J., Christian, S. J., and Ma, T., "A Model for the Investigation of Temperature, Heat Flow and Friction Characteristics During Engine Warm-Up," Society of Automotive Engineers, SAE Paper 931153, 1993.

[22]Kaplan, J. A., and Heywood, J. B., "Modeling the Spark Ignition Engine Warm-Up Process to Predict Component Temperatures and Hydrocarbon Emissions," Society of Automotive Engineers, SAE Paper 910302, 1991.

[23]Bohac, S. V., Baker, D. M., and Assanis, D. N., "A Global Model for Steady State and Transient S.I. Engine Heat Transfer Studies," Society of Automotive Engineers, SAE Paper 960073, 1996.

[24]Maloney, P. J., and Olin, P. M., "Pneumatic and Thermal State Estimators for Production Engine Control and Diagnostics," Society of Automotive Engineers, SAE Paper 980517, 1998.

[25]Incropera, F. P., and DeWitt, D. P., *Fundamentals of Heat and Mass Transfer*, Wiley, New York, 1990.

[26]Taylor, C. F., and Toong, T. Y., "Heat Transfer in Internal Combustion Engines," American Society of Mechanical Engineers, ASME Paper 57-HT 17, 1957.

[27]Yoo, I. K., Simpson, K., Bell, M., and Majkowski, S., "An Engine Coolant Temperature Model and Application for Cooling System Diagnosis," Society of Automotive Engineers, SAE Paper 2000-01-0939, 2000.

[28]Smith, L. R., and Franchek, M. A., "Nonlinear Modeling and Robust Control of a Single Cylinder I.C. Engine for Hybrid Vehicle Applications," Proceedings of the American Society of Mechanical Engineers ICEME, 1999.

[29]Howard, J. R., and Sutton, A. E., "An Analogue Study of Heat Transfer Through Periodically Contacting Surfaces," *International Journal of Heat and Mass Transfer*, Vol. 13, pp. 173–183.

[30]Mckinzie, D. J., Jr., "Experimental Confirmation of Cyclic Thermal Joint Conductance," AIAA Paper 70-853, 1970.

[31]Heisler, H., *Advanced Engine Technology*, Society of Automotive Engineers, Hodder Headline Group, 1995.

[32]Yang, L. C., Hamada, A., and Ohtsubo, K., "Engine Valve Temperature Simulation System," Society of Automotive Engineers, SAE Paper 2000-0100564, 2000.

[33]Moses, W. M., and Dodd, N. C., "Heat Transfer Across Aluminum/Stainless-Steel Surfaces in Periodic Contact," *Journal of Thermophysics and Heat Transfer*, Vol. 4, No. 3, 1990, pp. 396–398.

[34]Taylor, C. F., and Landy, E., *The Internal Combustion Engine in Theory and Practice: Combustion, Fuels, Materials, and Design*, Vol. 2, MIT Press, Cambridge, MA, 1985.